

## NUMERICAL INVESTIGATION OF VERTICAL AXIS WIND TURBINE WITH TWIST ANGLE IN BLADES

Sahar NOORI<sup>1\*</sup> and Navid RANJBARAN

<sup>1</sup> Department of Aerospace Engineering, Amirkabir University, Tehran, IRAN

\*S\_noori@aut.ac.ir

### ABSTRACT

This paper reports on the numerical simulation of a vertical axis wind turbine with three straight NACA0015 airfoils. The aim is to investigate the effect of twist angle on output power coefficient of the turbine at angles of 15 and 30 degrees. Modelling and mesh generation steps are done in Gambit, and numerical simulations in Fluent in 2-dimensional transient state with different revolution speeds, using turbulent model due to large flow separation. In this study, sliding mesh method is used to rotate the airfoils. Numerical results obtained in this study have a good correlation with experimental data, showing that the best aerodynamic performance is achieved at twist angle of 15 degrees, located at 90% of chord length from leading edge.

### NOMENCLATURE

$A$	Swept area
$c$	Chord length
$c_d$	Drag coefficient
$c_l$	Lift coefficient
$c_t$	Tangential force coefficient
$c_n$	Normal force coefficient
$c_p$	Power coefficient
$c_m$	Moment coefficient
$N$	Number of blades
$R$	Radius of rotor
$u_\infty$	Free stream velocity
$F_n$	Normal force
$F_t$	Tangential force
$H$	Height of the wind rotor
$W$	Wind velocity
$L$	Lift
$D$	Drag
$\alpha$	Angle of attack
$\rho$	Density
$\gamma$	Twist Angle
$\lambda$	Tip speed ratio
$k$	Turbulence kinetic energy
$G_K$	Turbulence kinetic energy generation
$\varepsilon$	Dissipation rate
$\gamma$	Blade twist angle
$\mu_{\text{eff}}$	Effective viscosity
$\alpha_k$	Inverse effective Prandtl number by $k$
$\alpha_\varepsilon$	Inverse effective Prandtl number by $\varepsilon$
$\omega$	Angular velocity

### INTRODUCTION

Horizontal axis wind turbines (HAWT) are conventional wind turbines. In other hand, vertical axis wind turbines (VAWT) are new technology turbines and their applications are rapidly growing. The wind turbines are named in reference at the direction of their axis with respect to the ground, i.e. if the axis of the turbine is parallel to the ground, it is called HAWT, and if it is perpendicular to the ground, it is called VAWT. The rotor of VAWTs rotates independently of the wind direction and this is one of the most important advantages of this type of turbine, especially when the wind direction is highly variable. Another advantage of VAWTs is that their gearbox and generator can be positioned near to the level due to the vertical position of the turbine axis. This facilitates maintenance operations. Some VAWT are able to start automatically. That depends on the blade design and the wind velocity. Early studies concentrated on VAWTs with drag force while the attention of researchers has been recently shifted to VAWTs with lift force.

### AERODYNAMIC ANALYSIS OF WIND TURBINES

Though the straight-bladed VAWTs are simple in design, their aerodynamic analysis is quite complex. Different models have been proposed to predict the design and performance of Darrieus-type wind turbines. The most typical models are classified in three categories: momentum models, vortex models and cascade models.

Fig.1 shows tangential and normal forces as well as the direction of drag and lift forces with respect to the angle of attack.

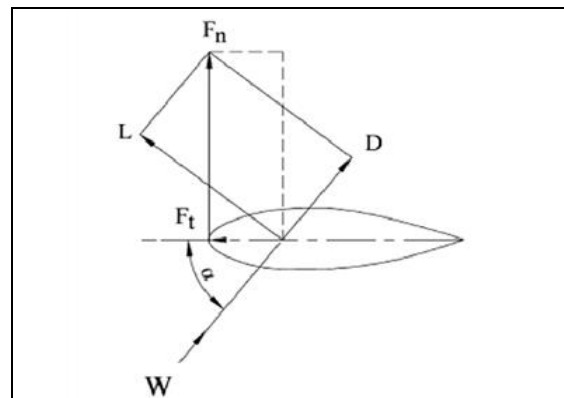


Figure 1: Forces on a blade in flow field.

According to fig. 1, the coefficients of tangential and normal forces are calculated as follows:

$$\begin{aligned} C_t &= C_l \cdot \sin\alpha - C_d \cdot \cos\alpha \\ C_n &= C_l \cdot \cos\alpha + C_d \cdot \sin\alpha \end{aligned} \quad (1)$$

The tangential and normal forces are defined as below:

$$\begin{aligned} F_t &= C_t \frac{1}{2} \rho c H W^2 \\ F_n &= C_n \frac{1}{2} \rho c H W^2 \end{aligned} \quad (2)$$

Average tangential force is derived from the following equation:

$$F_{ta} = \frac{1}{2\pi} \int_0^{2\pi} F_t(\theta) d\theta \quad (3)$$

Total output momentum is calculated by this equation:

$$M = N \cdot F_{ta} \cdot R \quad (4)$$

Turbine power, therefore, will be as:

$$P = M \cdot \omega \quad (5)$$

## PERFORMANCE PARAMETERS OF WIND TURBINES

The coefficient of momentum and power coefficient are the performance parameters of a wind turbine and are defined as below:

$$C_m = \frac{M}{\frac{1}{2} \rho u_\infty^2 A r} \quad (6)$$

$$C_P = \frac{P}{\frac{1}{2} \rho u_\infty^3 A} \quad (7)$$

Equations (6) and (7) are related to each other through the following relation:

$$C_m = \frac{C_P}{\lambda} \quad (8)$$

That  $\lambda$  is tip-speed ratio (TSR) derived from the following relation:

$$\lambda = \frac{r\omega}{u_\infty} \quad (9)$$

The power coefficient of a wind turbine is a function of TSR.

## GOVERNING EQUATIONS

In the process of analyzing Darrieus-type turbines, a mathematical demonstration of flow field within computational range is necessary for achieving a solution. The assumptions associated with incompressible, non-steady and Newtonian fluid as well as RNG k- $\epsilon$  turbulent model were used in the simulation of flow.

The choice of the turbulence models influences the resultant flow field and the computational resource and time required to achieve solutions. For HAWTs it was found that standard k- $\epsilon$  model gave inaccurate results after flow separation in the previous research done by Wolfe and Ochs. However, the RNG k- $\epsilon$  model is known to predict flow fields involving large flow separations more accurately so for the present task, RNG k- $\epsilon$  turbulence model was used. The flow equations are demonstrated in the following.

Continuity Equation:

$$\frac{\partial}{\partial x_i} (\overline{\rho u_i} + \overline{\rho' u_i'}) = 0 \quad (10)$$

Momentum Equation:

$$\begin{aligned} \frac{\partial}{\partial t} (\overline{\rho u_i}) + \frac{\partial}{\partial x_i} (\overline{\rho u_i u_j}) + \rho (2\overline{\omega} \times \overline{u_i} + \overline{\omega} \times \overline{\omega} \times \vec{r}) \\ = \frac{\partial \overline{P}}{\partial x_i} + \frac{\partial (\tau_{ij})_{\text{eff}}}{\partial x_j} \end{aligned} \quad (11)$$

In this state, the momentum equation includes two additional terms: Coriolis acceleration and centripetal acceleration.

The transport equations considerate for the turbulence quantities from RNG k- $\epsilon$  model are described by Equations (12) and (13).

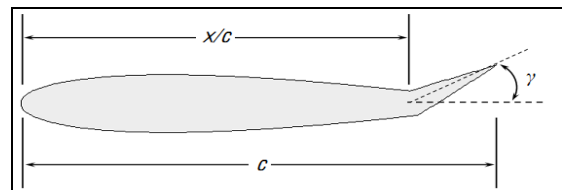
$$\frac{\partial (\rho k)}{\partial t} + \frac{\partial (\rho k u_i)}{\partial x_i} = \frac{\partial (\alpha_k \mu_{\text{eff}} \frac{\partial k}{\partial x_j})}{\partial x_j} + G_k - \rho \epsilon \quad (12)$$

$$\begin{aligned} \frac{\partial (\rho \epsilon)}{\partial t} + \frac{\partial (\rho \epsilon u_i)}{\partial x_i} = \frac{\partial (\alpha_\epsilon \mu_{\text{eff}} \frac{\partial \epsilon}{\partial x_j})}{\partial x_j} \\ + C_{1\epsilon} \frac{\epsilon}{k} G_k - C_{2\epsilon} \rho \frac{\epsilon^2}{k} - R_\epsilon \end{aligned} \quad (13)$$

Where  $G_k$  represents the generation of turbulent kinetic energy due to mean velocity gradients, and  $\alpha_k$  and  $\alpha_\epsilon$  are Prandtl numbers for k and  $\epsilon$ , respectively.

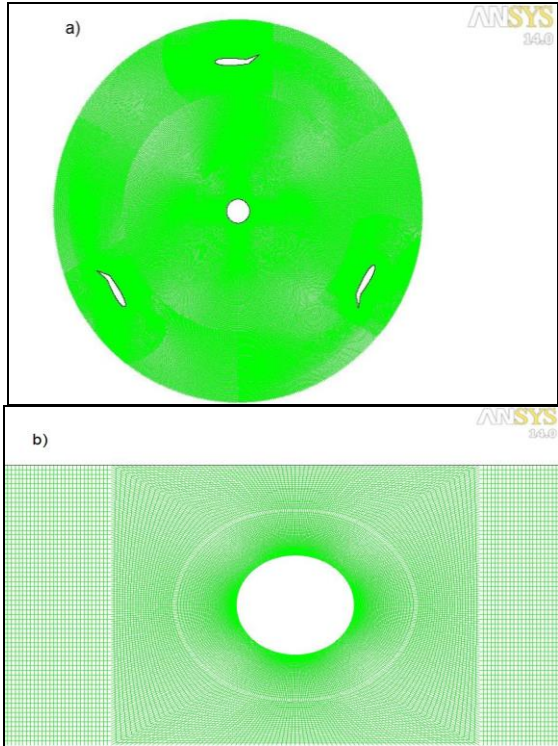
## COMPUTATIONAL NMODEL AND GRID GENERATION

Fig. 2 shows the geometry of one of the blades used in the numerical analysis with a twist angle of  $\gamma$  located at  $\frac{x}{c}$  to leading attack.



**Figure 2:** Blade geometry with a twist angle located at trailing edge of airfoil.

Gambit was used to generate the grid. All the elements of this grid are structured elements. In order to increase the accuracy, the mesh density is high near the surface of the blades. Fig. 3 shows the generated grid structure.



**Figure 3:** Computational grid:

a) rotating sub-domain, and b) stationary sub-domain

Table 1 shows the geometrical variables for each configuration of VAWT.

Rotor	$C[m]$	$\gamma$ [deg]	$x/c$ [-]
A	0.05	15	0.7
B	0.05	30	0.7
C	0.05	15	0.8
D	0.05	30	0.8
E	0.05	15	0.9
F	0.05	30	0.9
G	0.05	0	1.0

**Table 1:** Different geometries of airfoils.

Table 1 represents an early parametric study, which will identify more and less sensitive geometric parameters for future studies aimed more towards optimization and other design changes.

### GRID INDEPENDENCY

In a numerical analysis, an ideal solution is achieved when the solutions are independent of the grid. Table 2 shows the coefficient of momentum for  $\gamma = 0^\circ$ . The difference between coefficients in stages 4 and 5 was below 5%. A grid with 114050 cells was selected for the model.

Refining level	Number of elements	$C_m$
1	14509	0.002
2	42190	0.026
3	70262	0.056
4	106105	0.034
5	114050	0.034

**Table 2:** Moment coefficient in terms of the number of elements.

### BOUNDARY CONDITIONS

Fig. 4 shows boundary conditions. An inlet velocity of 8 m/s was considered as the inlet boundary condition while the pressure outlet was considered as the outlet boundary condition. For airfoils, non-sliding wall was defined as the boundary condition. To apply the sliding mesh, boundary condition was defined as the interface between rotating and stationary zones. The top and bottom of the domain are defined as non-slip walls. It should be noted that the relative dimension of overall domain size relative to turbine size is suitable as used by K.M. Almomhamadi and D.B. Ingham.

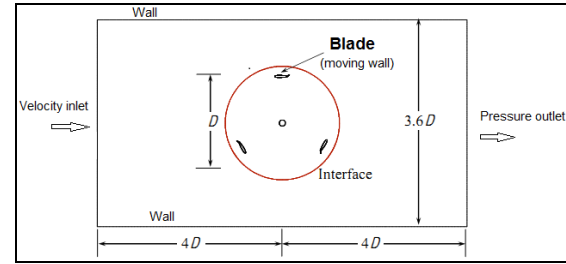


**Figure 4:** Boundary conditions for a straight-bladed VAWT turbine.

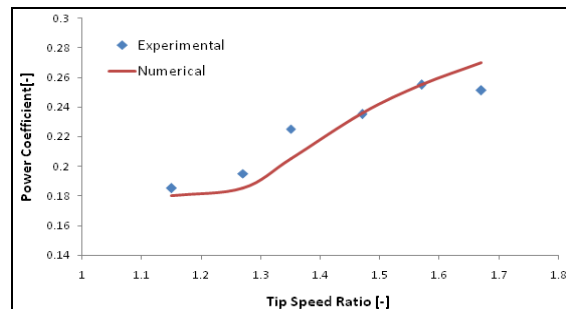
### RESULTS

This section analyzes the numerical simulation results and compares them with experimental data.

#### VALIDATION OF NUMERICAL SIMULATION

Bravo et al. developed an experimental analysis of a H-type Darrieus VAWT with a diameter of 2.5m and a height of 3m. The blades have a NACA0015 profile with a chord length of 0.4m.

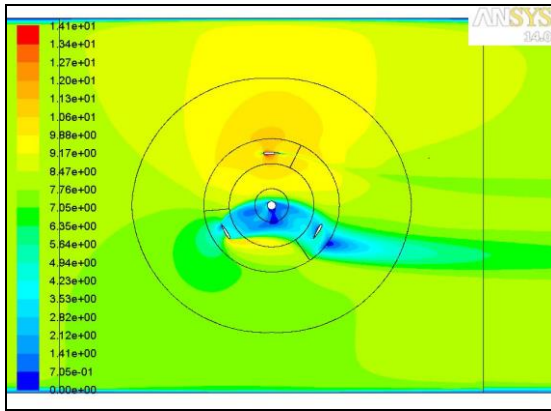
Fig.5 compares the power coefficients of numerical simulation and experimental data. It can be observed that the numerical results present a good prediction of the wind turbine performance compared to experimental data.



**Figure 5:** Comparison of numerical and experimental data.

## VELOCITY CONTOURS

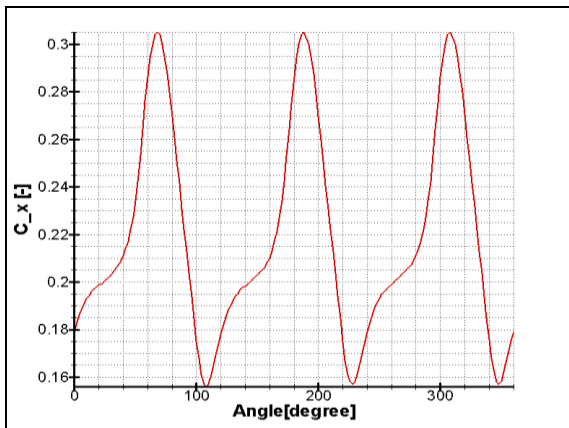
Fig. 6 shows velocity contours for  $\lambda=0.5$ . Flow separation and the creation of vortex current due to the rotation of blade can be seen in this figure. Velocity range is  $0 \leq V \leq 14.1$  m/s.



**Figure 6:** Velocity contours m/s at the 10th rotation of rotor G.

## FORCES ON BLADES

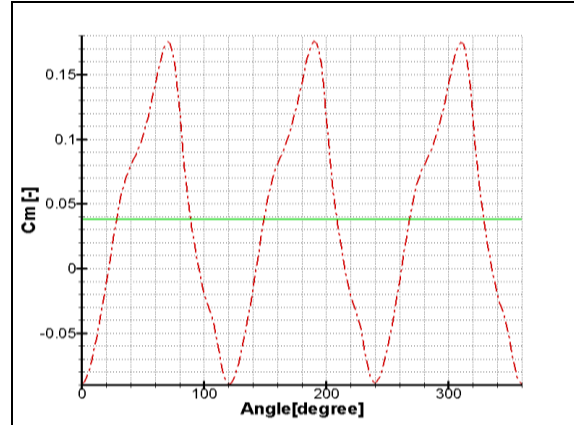
Fig.7 shows the coefficient of horizontal velocity exerting on blades during rotation for  $\lambda=0.5$ . The frequent behavior of this force is of a flow nature around a VAWT. This behavior will not be perfect due to vortex currents resulting from the rotation of blades.



**Figure 7:** Horizontal force coefficient versus rotation angle (Rotor\_A).

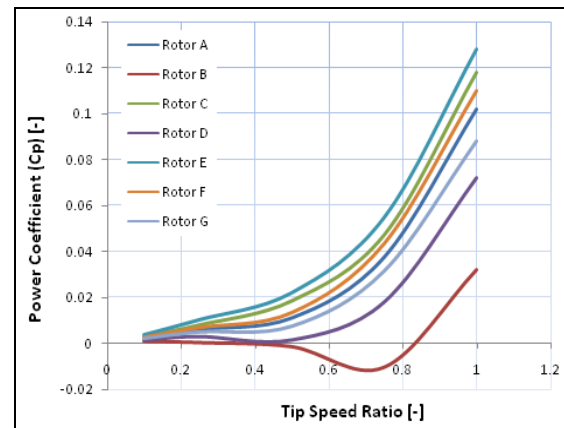
## COEFFICIENT OF MOMENTUM AND OUTPUT POWER COEFFICIENT

Fig. 8 shows the coefficient of momentum derived from the numerical simulation for  $\lambda=0.5$  and rotor C. This coefficient becomes minimum at three positions of blades (i.e. angles of  $120^\circ$ ,  $240^\circ$  and  $360^\circ$ ), that is a negative and non-ideal solution. At these positions, one of the blades is positioned at the rotation angle of zero with the drag force as the main force exerting on the blade in an opposite direction to rotation direction. The average coefficient of momentum is  $C_{m_{Ave}} = 0.037$ .



**Figure 8:** Coefficient of momentum versus rotation angle.

Fig. 9 shows average power coefficient versus tip-speed ratio.



**Figure 9:** Power coefficient versus TSR.

According to figure 9, in all states power coefficient becomes maximum for  $\lambda=1$  while it is zero for  $\lambda=0$  implying no rotation of blades. For rotor B, power coefficient becomes negative in some ranges of TSR. In this case, the wind not only does not help blades to rotate but also it serves as an obstacle.

## CONCLUSION

The best aerodynamic performance of a wind turbine occurs at  $\frac{x}{c} = 0.9$  and  $\gamma = 15^\circ$ , while the worst one occurs at  $\frac{x}{c} = 0.7$  and  $\gamma = 30^\circ$ . It can be argued, therefore, that the aerodynamic performance of straight-bladed VAWTs under the influence of twist angle increases as the ratio of  $\frac{x}{c}$  increases and decreases as the twist angle rises from  $15^\circ$  to  $30^\circ$ , resulting in the increase of drag force that generates a torque opposite to turbine rotation direction.

## REFERENCES

- JAMES, T. and YING, A.C., (1988), "A new technique for producing stencils", *Proc. Int. Cong. on Stencils*, ABCD, Melbourne, Australia, February 29-31.
- LUKE T., (1988), "A new technique for Stencil publishing", *J. Stencils*, **5**, 179-221.
- HAU E., (2006), "Wind Turbines: Fundamentals, Technologies, Applications, Economics" 2nd Edition, Springer, Berlin, 783p.
- HABTAMU, B. , (2011), "Effect of Camber Airfoil on Self Starting of Vertical Axis Wind Turbine", *Journal of Environmental Science and Technology*, **4**, pp 302-312.
- BURTON, T., (2001), "Wind Energy Handbook", John Wiley and Sons, 617p.
- FARTAJ, A., (2008), "Aerodynamic Models For Darrieus-Type Straight Bladed Vertical Axis Wind Turbines", *Renewable And Sustainable Energy Reviews*, **12**, pp1087-1109.
- Wolfe EP., Ochs SS., (1997), "CFD calculations of S809 aerodynamic characteristics" AIAA aerospace sciences meeting.
- Ansys. Fluent Theory Guide, (2009), Ansys Inc.
- CHOUDHURY , D., (1993), " Introduction to the Renormalization Group Method And Turbulence Modeling ", Fluent Incorporated, 70p.
- Ansys, Gambit, (2009), Ansys Inc.
- HOWELL, R., (2010). "Wind Tunnel And Numerical Study Of a Small Vertical Axis Wind Turbines", *Renewable Energy*, **35**, pp 412-422.
- K.M.Almohammadi, D.B.Ingham, L.Ma. Pouy Kashan, (2013), "Computational fluid dynamics (CFD) mesh independency techniques for a straight blade vertical axis wind turbine", *Energy* **58** , 483-493.
- R. BRAVO, TULLIS, S., and ZIADA, S., (2007), "Performance Testing of a Small Vertical Axis Wind Turbine", *Conference on Applied Mechanics*, **21**, pp 2-3.